submitted to the Journal of Chemical Physics

A Computationally-Efficient Exact Pseudopotential Method. II. Application to the Molecular Pseudopotential of an Excess Electron Interacting with Tetrahydrofuran (THF)

C. Jay Smallwood, Ross E. Larsen, and Benjamin J. Schwartz*
Department of Chemistry and Biochemistry, UCLA
Los Angeles, CA 90095-1569

(Dated: August 5, 2005)

Abstract: In the preceding paper, we presented an analytic reformulation of the Phillips-Kleinman (PK) pseudopotential theory. In the PK theory, the number of explicitly treated electronic degrees of freedom in a multi-electron problem is reduced by forcing the wavefunctions of the few electrons of interest (the valence electrons) to be orthogonal to those of the remaining electrons (the core electrons); this results in a new Schrödinger equation for the valence electrons in which the effects of the core electrons are treated implicitly via an extra term known as the pseudopotential. Although this psuedopotential is nonlocal and must be evaluated iteratively, our reformulation of the theory allows the exact pseudopotential to be found without ever having to evaluate the potential energy operator, providing enormous computational savings. In this paper, we present a detailed computational procedure for implementing our reformulation of the PK theory, and we illustrate our procedure on the largest system for which an exact pseudopotential has been calculated, that of an excess electron interacting with a tetrahyrdrofuran (THF) molecule. We discuss the numerical stability of several approaches to the iterative solution for the pseudopotential, and find that once the core wavefunctions are available, the full e^-–THF pseudopotential can be calculated in less than 10 s on a relatively modest single processor. We also comment on how the choice of basis set affects the calculated psuedopotential, and provide a prescription for correcting unphysical behavior that arises at long distances if a Gaussian basis set is used. Finally, we discuss the effective e^-–THF potential in detail, and present a multi-site analytic fit of the potential that is suitable for use in molecular simulation.

I. INTRODUCTION

There are a very limited number of systems of interest in chemistry and condensed-matter physics that have only a few electrons; however, few-electron systems are currently the boundary for exact quantum mechanical calculations. As such, it is imperative to find approximations to the many-electron problem that provide for accurate wavefunctions and energies but avoid explicit computation of most of the electrons. The standard approach to reduce the number of electrons is to first separate the many-electron system into core and valence electrons. This separation is based on the fact that core electrons are typically static during chemical processes so that by treating the core-valence and core-core electron interactions approximately, an exact calculation can be done for the small number of valence electrons while still retaining the important physics of the system. One of the most common approximations is to implicitly include the effects of the core electrons on the valence electrons by adding a new potential, known as a pseudopotential, to the valence electron Hamiltonian. Pseudopotentials have been used in a wide variety of fields ranging from solid-state electronic structure calculations [1] to mixed quantum/classical molecular dynamics [2–6].

Although pseudopotentials are often developed empirically [1, 7], it is possible to rigorously derive a pseudopotential based on quantum mechanical theory; such a formalism was first developed by Phillips and Kleinman (PK) [8] and has been extended by others (see e.g. Ref. [7] and references therein). The PK theory provides a quantum mechanical solution for the valence electrons by solving a modified eigenvalue equation that includes a non-local pseudopotential term. Historically, however, use of the PK theory has been plagued by two main implementation issues. First, the theory requires accurate solutions for the core electron wavefunctions. Second, even if the core electron wavefunctions are available, solving for the valence electrons in the modified eigenequation is computationally expensive because the non-local pseudopotential necessitates an iterative solution of the PK equation. Therefore, several approximate schemes have been used in lieu of calculating the exact pseudopotential, including the use of approximate Hamiltonians [9] and the use of model wavefunctions for the core electrons [10, 11]. The use of model wavefunctions works particularly well for systems where there is a great deal of intuition about the shape of the core wavefunctions, such as with atomic orbitals, but in molecular systems where the core wavefunctions are more complex, this type of approximation rapidly loses accuracy. Thus, for molecular systems, accurate results require a direct solution of the PK equation; unfortunately, complex molecular systems are the very ones for which direct application of the PK formalism is the least computationally feasible.

In the preceding paper [12], we presented an analytically exact reformulation of the PK pseudopotential theory. The principal advantage of our reformulation is that it is highly computationally efficient: our method avoids the need to calculate the potential energy operator and its two-electron integrals during the self-consistent solution of the PK eigenequation, thus eliminating what is the rate-limiting step for solving any many-electron problem. In addition, our new formalism allows us to build a geometric understanding of the PK theory and provides a straightforward means to extend the theory beyond the frozen core approximation [7, 9, 13]. In this paper, we illustrate the implementation of our formalism for a complex molecular pseudopotential; in particular, we compute the exact PK pseudopotential for a single excess electron interacting with a (closed-shell) tetrahydrofuran (THF) molecule. We chose this system for two main reasons. First, this system is an excellent testbed for demonstrating the advantages of our method: there is little intuition by which to approximate the THF core molecular wavefunctions, and to the best of our knowledge, there has been no molecule as large as THF for which the exact pseudopotential has been calculated. In fact, we will demonstrate below that with our new formalism, calculation of the THF-electron pseudopotential is computationally trivial, opening the way to molecules of much greater complexity. Second, our group has a long-standing interest in experiments and nonadiabatic mixed quantum/classical molecular dynamics simulations of both solvated electrons [2, 14, 15] and sodium anions [3, 16–20] in liquid THF. In the past [2], we have specified how the quantum mechanical electron interacts with the classical THF molecules in simulations by using an empirical pseudopotential based on physical ideas presented by Berne and co-workers [21]. In future work, we will compare mixed quantum/classical electron-THF simulations using the exact pseudopotential presented here to those using the empirical pseudopotential presented in our previous work; the results should allow us to learn a great deal about how accurate a pseudopotential must be to obtain reliable results in mixed quantum/classical molecular simulations.

The rest of this paper is organized as follows. In Section II, we summarize our formalism in the context of providing a computationally efficient procedure for the calculation of exact pseudopotentials. We then discuss the numerical implementation of our procedure for the specific case of an excess electron interacting with a THF molecule. Next, we address issues concerning how the calculated pseudopotential depends on the choice of basis set, and we present the full calculated exact e^-–THF effective potential in detail. In Section III we describe how we fit the resulting pseudopotential to a set of analytic functions for use in molecular simulation and comment on the accuracy of our fit. We conclude in Section IV.

II. CALCULATION OF THE EXACT ELECTRON-THF PSEUDOPOTENTIAL

A. Review of the Pseudopotential Formalism

Since we will be applying a new formalism for the calculation of exact pseudopotentials, we begin our discussion by giving a brief description of the underlying theory; a full description of the theory can be found in the preceding paper, Reference [12]. The goal of pseudopotential theory is to reduce the number of explicitly treated electronic degrees of freedom (in our case, to one valence electron) by implicitly including the effects of the lower-lying core electrons (which we define as those electrons that remain approximately static during the physical process of interest) as an additional potential term to the Hamiltonian. As discussed in Ref. [12], constructing the pseudopotential is equivalent to writing the valence electron wavefunction in a basis that has been made orthogonal to the core-electron wavefunctions. The core and valence electronic wavefunctions are the eigenvectors of the Hamiltonian, $\hat{H} = \hat{T} + \hat{U}$. The core-electron eigenstates are given by,

$$\hat{H}|\psi_i\rangle = \epsilon_i|\psi_i\rangle \qquad (i = 1, ncore), \tag{1}$$

where *ncore* is the total number of core electrons and the valence electron wavefunction is given by,

$$\hat{H}|\psi_v\rangle = \epsilon|\psi_v\rangle. \tag{2}$$

If the valence electron is written in a basis for which each basis function has been *a priori* orthogonalized to every core-electron wavefunction, then Eqn. 2 becomes [8],

$$\hat{H}|\phi\rangle + \sum_{i=1}^{ncore} |\psi_i\rangle\langle\psi_i|\epsilon - \hat{H}|\phi\rangle \equiv [\hat{H} + \hat{V}_p]|\phi\rangle = \epsilon|\phi\rangle. \tag{3}$$

This is the Phillips-Kleinman pseudopotential equation. It has the same structure as Eqn. 2 except that there is an additional potential term, the pseudopotential, $\hat{V}_p$. The ground state solution to this effective Hamiltonian, $\hat{H} + \hat{V}_p$, is called the pseudo-orbital, $|\phi\rangle$, and has an energy identical to that of the valence electron. The relationship between the pseudo-orbital and the valence electron arises from the pre-orthogonalization of the basis set,

$$|\psi_v\rangle = |\phi\rangle - \sum_{i=1}^{ncore} |\psi_i\rangle\langle\psi_i|\phi\rangle. \tag{4}$$

Thus, the valence electron solutions to the PK pseudopotential equation are guaranteed to be orthogonal to the core electrons. Moreover, since $|\phi\rangle \rightarrow |\psi_v\rangle$ outside the core electron region, solving Eqn. 3 for the pseudo-orbital suffices to solve the problem away from the core.

The pseudo-orbital solution to Eqn. 3, however, is not unique [22]; thus, we can impose an additional constraint that does not affect the orthogonality between the valence and core electron wavefunctions. By choosing a constraint in which the expectation value of the pseudo-orbital is extremized with respect to an arbitrary operator, $\hat{F}$, we can find a unique solution for the pseudo-orbital by solving,

$$\hat{H}|\phi\rangle + \sum_{i=1}^{ncore} |\psi_i\rangle\langle\psi_i|\epsilon - \hat{H} + \hat{F} - \langle\hat{F}\rangle|\phi\rangle = \epsilon|\phi\rangle, \tag{5}$$

where $\langle\hat{F}\rangle = \langle\phi|\hat{F}|\phi\rangle/\langle\phi|\phi\rangle$ is the expectation value of $\hat{F}$ for the pseudo-orbital $|\phi\rangle$. As discussed in the Introduction, Eqn. 5 is computationally expensive to solve, which has limited its use and forced researchers to work with various approximate schemes. In Ref. [12], however, we showed that if we choose to minimize the expectation value of the kinetic energy operator, $\hat{T}$, instead of solving Eqn. 5, the same unique pseudo-orbital $|\phi\rangle$ can be calculated by solving,

$$|\phi\rangle = |\psi_v\rangle + \sum_{i=1}^{ncore} \frac{\langle\psi_i|\hat{T}|\phi\rangle}{\langle\hat{T}\rangle}|\psi_i\rangle. \tag{6}$$

The advantage of this choice of constraint is that the self-consistent solution for the pseudo-orbital via Eqn. 6 entirely avoids the computation of the potential energy operator. Since the potential energy term involves the calculation of two-electron integrals, the evaluation of the potential energy is always the slow step in multi-electron calculations. In this paper, we will use kinetic-energy minimization to calculate the excess e$^-$–THF pseudopotential since our formulation with this choice removes the main computational bottleneck.

Once the unique pseudo-orbital has been calculated via Eqn. 6, it is straightforward to calculate the pseudopotential. For molecular simulations and other applications, however, what is most often needed is the total effective potential, U_{eff}, which includes the potential from the original Hamiltonian as well as the additional repulsive pseudopotential, $\hat{V}_p$, that arises from pre-orthogonalization. Unfortunately, the pseudopotential arising from the solution to Eqn. 6 is non-local, making its on-the-fly evaluation impractical for use in simulations. However, the fact that $|\phi\rangle$ is the ground-state solution to Eqn. 5 means that it is nodeless, allowing the total effective potential from the kinetic-energy-minimized pseudo-orbital determined from Eqn. 6 to be localized by,

$$U_{eff}^{local}(\mathbf{r}) = \frac{\langle\mathbf{r}|(\epsilon - \hat{T})|\phi\rangle}{\langle\mathbf{r}|\phi\rangle}. \tag{7}$$

So, if we choose to minimize the kinetic energy, our formalism allows us to entirely avoid calculating the potential energy operator after the initial step of finding the core and valence electron wavefunctions [12]. With all the pieces in place, we next illustrate how to apply this formalism to calculate the effective potential for a complex molecular system, namely an excess electron interacting with a THF molecule.

B. Computational Details in Solving for the THF-e$^-$ Pseudopotential

The first step in calculating the local effective potential for an excess electron interacting with a THF molecule was to find the core and valence electron wavefunctions, Eqns. 1 and 2, of THF. In line with previous work on molecular pseudopotentials, [9, 13, 23] we solved for the molecular orbitals (MOs) of THF using closed-shell Hartree-Fock theory [24] within the frozen-core approximation [25] (i.e. we assumed that the closed-shell core electrons are not altered by the presence of the excess electron). We solved for all of the molecular orbitals of the THF molecule using the Gaussian 98 program [26] with a restricted Hartree-Fock Hamiltonian and a 6-31++g cartesian Gaussian basis set; for THF, this basis set contains 89 contracted Gaussian functions. Since our interest in developing the electron-THF pseudopotential is to employ it in mixed quantum/classical simulations of liquid THF, we chose the geometry of the THF molecule in our calculations, shown in Figure 1, to match that of the classical THF model used in the Monte Carlo simulations of Jorgenson and co-workers [27].

Even though the fully-optimized structure of THF is bent (and at finite temperature undergoes pseudorotation), we calculated the pseudopotential for a THF molecule that is constrained so that all four C atoms and the O atom are co-planar for the following reasons. First, Jorgenson and co-workers found that both planar and pseudorotating bent models of THF produced identical solvent packing, so that the use of the planar model is justified for simulations of the liquid [27]. Second and perhaps more importantly, approximating the THF molecule as planar avoids the difficulty of having to calculate a different pseudopotential for every possible bent geometry. Since we plan to employ Jorgenson and co-workers' planar model of THF for mixed quantum/classical simulations, we calculated the electron-THF pseudopotential for this geometry both for internal consistency and to facilitate comparisons with our previous simulations [2]. The THF geometry we used to calculate our pseudopotential does, however, include one important structural difference from Jorgenson and co-workers' planar model. Their model employed united atoms for the methylene groups to avoid explicit inclusion of the hydrogen atoms [27], but as we demonstrate below in Section II D, inclusion of the hydrogen atoms is essential to correctly reproduce the exact pseudopotential. Thus, even though it will require calculating the positions of hydrogen atoms that are not present in the classical THF simulation model, we must include the hydrogen atoms in the calculation of the pseudopotential for our upcoming simulations. To determine the positions of the hydrogen atoms, we calculated the energy-minimized electronic structure of the THF molecule by first constraining the heavy atoms of the backbone to match the geometry of the planar Jorgensen model and then allowed the positions of the hydrogen atoms to optimize. The 20 occupied core MOs and the LUMO (which is the valence electron within the static-exchange approximation) of this hydrogen-optimized planar structure are what was used to calculate the pseudopotential.

With the MOs of THF in hand, we next calculated the pseudo-orbital by solving Eqn. 6. To solve this equation, we needed to find the coefficients for $|\phi\rangle$ in terms of our chosen basis set. Since $\langle\hat{T}\rangle$ is a functional of $|\phi\rangle$, Eqn. 6, like Eqn. 5 (with the choice $\hat{F} = \hat{T}$), must be solved self-consistently. As with the iterative solution to any self-consistent equation, the numerical convergence of solving Eqn. 6 is quite sensitive to methodology. The first approach we tried was to expand each of the molecular orbitals in terms of the 6-31++g Gaussian basis set and then solve for the pseudo-orbital by iterating with a simple successive approximation,

$$|\phi_{new}\rangle = |\psi_v\rangle + \sum_{i=1}^{ncore} \frac{\langle\psi_i|\hat{T}|\phi_{old}\rangle}{\langle T\rangle_{old}} |\psi_i\rangle, \tag{8}$$

This approach, however, was extremely numerically unstable and did not converge for a variety of starting guesses. Instead, we found that we could achieve a stable numerical solution for the pseudo-orbital using an iterative matrix-inversion scheme to solve the rearranged equation,

$$|\phi\rangle = \left[I - \frac{\hat{\Omega}\hat{T}}{\langle T\rangle}\right]^{-1} |\psi_v\rangle \equiv \hat{M}^{-1}|\psi_v\rangle \tag{9}$$

where $\hat{T}$ is the kinetic energy operator and $\hat{\Omega} = \sum_{i=1}^{ncore} |\psi_i\rangle\langle\psi_i|$ is the projection operator onto the occupied core MOs. To iteratively solve Eqn. 9, we expanded the matrix in terms of our contracted Gaussian basis set, solved the linear matrix equation, $\hat{M}|\phi\rangle = |\psi_v\rangle$ using LAPACK routines [28], and used the resulting coefficients for $|\phi\rangle$ to form the matrix for the next iteration. (Note that the matrix inversion written in Eqn. 9 is only formal; in practice, only the linear matrix equation is solved on each iteration.) For our convergence criterion, we chose that the values of the basis set coefficients for $|\phi\rangle$ on successive iterations did not change within machine precision. For our choice of the 6-31++g basis set, using a 90% LUMO starting guess on a single Athlon AMD 1.3 GHz serial processor, it took less than ten seconds for the solution of Eqn. 9 to converge. In addition to the rapid convergence, the solution to Eqn. 9 is robust. For example, although it is typical for the LUMO to comprise $sim90\%$ of the pseudo-orbital [7, 8, 22], as we have found for THF, wildly unphysical starting guesses (e.g. assuming that the pseudo-orbital was composed 90% of lowest energy symmetry-allowed core orbital) still converged within ten iterations. Now that we have obtained the pseudo-orbital coefficients, the spatially-localized effective potential, described in more detail below in Section II D, can be calculated directly using Eqn. 7.

C. Numerical Issues Resulting from Choice of Basis Set

The computational procedure for solving Eqn. 6 as presented above is, in principle, independent of the basis set chosen to represent the core MOs. All that is needed are the coefficients of the core and valence electron wavefunctions and the kinetic energy matrix in that basis representation. However, we found two difficulties in calculating the THF-e^- effective potential that resulted directly from the choice of basis. In this subsection, we discuss both of these difficulties and how they can be avoided, and we compare our choice of basis set to that in previous molecular pseudopotential work.

Perhaps unsurprisingly, the first issue that arose is that the numerical solution of Eqn. 9 to find the pseudo-orbital was dependent on the quality of the basis set. As pointed out above, the pseudo-orbital is the ground-state solution to Eqn. 5 and thus should be nodeless. However, when we calculated the pseudo-orbital by iterating Eqn. 9 using a 6-31g basis set, which is localized to the molecular frame, the resulting solution contained nodes. But, when we switched to the 6-31++g basis set, which includes diffuse functions at every atomic site, a nodeless solution was found. The inclusion of diffuse functions in calculating the exact pseudopotential is critical: the solution we are seeking is that of an excess electron that resides in the LUMO of the THF molecule, which has significant diffuse character. Other researchers [23] have used even more extensive basis sets to calculate molecular pseudo-orbitals, but no tests were performed to investigate whether or not the extra basis functions were necessary for accuracy. For the THF-e^- system, we found that the inclusion of extra diffuse functions or the use of larger basis sets than 6-31++g did not significantly change either the LUMO energy or the general LUMO shape. Thus, for THF, the

6-31++g basis provided the optimal compromise between accuracy and computational expense. Of course, a larger basis set will provide more accuracy in regions far from the molecular core, but for applications in molecular simulation, the details of the pseudopotential far from the core are not likely to be terribly important as long as the psuedopotential has the correct asymptotic form (e.g., the $1/r^3$ decay of the molecular dipole).

The second issue that arose in our choice of basis set had to do with the functional form of the basis functions rather than their diffuse nature. When the local effective potential, Eqn. 7, is expressed as a function of spatial coordinates, both $\hat{T} = -\frac{1}{2}\hat{\nabla}^2$ and $|\phi\rangle$ are expanded in terms of the contracted Gaussian basis functions. It turns out that this choice of basis causes the local effective potential to diverge at large distances, as shown for a particular 1-D cut through the potential in Figure 2.

The fact that the pseudo-orbital in this basis must decay in a Gaussian manner at large distances leads to a quadratic divergence of the localized pseudopotential, $U_{eff}^{local} \propto r^2$; mathematically, this divergence arises because an asymptotically-decaying Gaussian wavefunction is associated with a harmonic potential. To remove this unphysical divergence of the pseudopotential, we can take advantage of the fact that $|\phi\rangle \rightarrow |\psi_v\rangle$ as we move away from the molecular region where the core orbitals decay to zero. Since the true effective potential should approach the Coulomb term for the LUMO outside the core MO's where exchange is negligible, we can join the effective potential found using Eqn. 7 (Fig. 2A, solid curve) with the LUMO Coulomb potential (Fig. 2A, dashed curve) wherever the two potentials cross outside the core region. A simple cutoff boundary for switching one potential into the other cannot be used since there are some intersections of the two potentials that must be excluded. But, we have developed a simple recipe for choosing the proper intersection at which to switch the two potentials; Figure 2 shows that before the short-range effective potential begins its harmonic divergence, it dips below the long-range LUMO Coulomb potential and then recrosses the long-range potential as it diverges. We chose to switch the effective potential to the long-range LUMO Coulomb potential at the closest crossing to the THF center of mass. Although this switching introduces a kink, the kink is negligible relative to the natural spatial variation of the overall molecular potential. Moreover, since we fit the exact potential to an analytic function, as described below in Section III, this kink will not exist in the final functional form representing the potential that will be used in molecular simulations.

D. The Exact THF-e$^-$ Effective Potential

With our choice of the 6-31++g basis and our procedure from the previous subsection that assures that the pseudopotential has the correct asymptotic form, we calculated the effective potential of an excess electron interacting with a THF molecule on an evenly spaced 64^3 cubic grid spanning -10 a_0 to 10 a_0 on a side, where $a_0 = 0.529$ Å is the Bohr radius. Representative 2-D cuts through the full 3-D effective potential are shown in Figures 3 and 4; the origin in both of these figures is set at the center of mass of the THF molecule, and the orientation of the THF backbone for each cut is shown in the top left corner of each panel.

Figure 3 shows two slices of the effective potential in planes parallel to the molecular backbone; panel A shows a cut 0.16 a_0 above the THF plane, and panel B shows a cut 0.48 a_0 above the molecular plane. The cut directly through the molecular plane is not shown since the potential is completely dominated by features centered at the atom sites that act to obscure most of the other details of the potential. The first thing to note from Fig. 3 is that the shape of effective potential is quite complex. In fact, it is evident in both panels of Fig. 3 that there are several features of the effective potential that are centered on neither the atomic sites nor the molecular bonds. The presence of such features highlights the importance of using the exact pseudopotential formalism instead of attempting to model the core MO electronic structure: model potentials based on atom-site and mid-point contributions (which both we [2] and others [21] have used in previous work) do not necessarily incorporate the appropriate physics. The next feature of the effective potential worth noting upon inspection of Fig. 3 is the strongly repulsive spikes near each atomic center. The presence of these repulsive features makes good physical sense: The purpose of the pseudopotential is to force orthogonality between the excess electron and the electrons in the core MOs, including the deeply buried atomic core orbitals on each atom in the molecule. Thus, the strong repulsive feature seen at the oxygen site in Fig. 3A prevents the excess electron from collapsing onto the lowest MO of the THF molecule – the oxygen 1s atomic orbital. The two strong repulsive features located to either side of the oxygen site show a similar repulsion that is likely due to the enforced orthogonality with the electrons in the oxygen lone pairs. The fact that these repulsive spikes originate primarily from repulsion from the atomic core orbitals is verified in Fig. 3B, which shows that by 0.48 a_0 above the molecular plane, there is no longer any strong repulsion from the oxygen atomic site. Indeed, a comparison of the two panels shows that the effective potential around the oxygen site is a compact repulsive ball centered in a larger attractive shell. The two panels also make it apparent that the effective potential near each carbon atomic site has a p-like feature with the repulsive lobe pointing away from the molecule.

Figure 4 shows the calculated effective potential from another perspective, this time in a cut perpendicular to the molecular plane near the β-hydrogen sites; the backbone orientation is shown in the top left corner of the figure. A comparison of Figures 3 and 4 shows that the spatial extent of the various features in the effective potential is not the same in the molecular plane as above and below the plane. But more importantly, Figure 4 shows that in addition to the carbon and oxygen atoms, the hydrogen atoms also produce well-defined features in the effective potential. The H atom features are attractive for the excess electron, which is perhaps not surprising given that the electronic structure of the planar THF molecule has essentially bare hydrogens (the Mulliken charge for the H atoms from the Gaussian 98 calculation is close to $+1$). Since repulsive terms in the effective potential arise from orthogonality constraints with core MOs, in regions where there is little core electron density, the attractive nuclear terms will dominate. The fact that the hydrogen atoms make a significant contribution to the total effective potential indicates that the use of a united atom approach will sacrifice accuracy; there is clearly a need to specifically include the hydrogen sites to correctly describe the interaction. Given the nature of the carbon-hydrogen chemical bond, it would seem that the pseudopotential for an excess electron interacting with virtually any hydrocarbon would also require explicit inclusion of the hydrogen atom sites.

III. FIT OF EFFECTIVE POTENTIAL FOR USE IN MOLECULAR SIMULATION

Our principal interest in the calculating the effective potential of an excess electron interacting with THF is to construct mixed quantum/classical molecular dynamics simulations of solvated electrons and sodium anions in liquid THF. The previous section presented the details of how we calculated the *exact* effective potential. Given the relatively large number of basis functions, the divergence of the potential caused by our choice of a Gaussian basis set, and the resulting need to taper the long-range potential to match that from the LUMO, on-the-fly calculation of the exact effective potential is simply too tedious to be practical for molecular simulation. Instead, we need an easily evaluable analytic function that closely approximates the effective potential for use in molecular dynamics calculations. The exact effective potential, which includes contributions from the five backbone atoms, the eight hydrogen atoms, and a few sites that are not associated with any of the atoms or bond midpoints, is sufficiently complex that a fairly large parameter space is required for an accurate fit. Thus, we chose to fit our effective potential to a function with a large number of free parameters even though such a complex nonlinear fit can be somewhat computationally demanding. However, the fit only has to be calculated once, and as long as the total number of parameters is similar to that used in simpler models, the increase in accuracy compensates for any additional cost to the actual molecular simulations.

We performed the fit using the unconstrained non-linear fitting routine *nlinfit.m* in the MATLAB 7, Release 14 Statistics Toolbox. The 47-parameter function to which we chose to fit our effective THF-e$^-$ potential, along with a summary of the best-fit parameters, is written in Table I. Our fit function is comprised of 19 different sites, and these sites fall into two different classes, atom-centered sites and sites not located on the molecular framework. If a function is centered on an atom site, the position vector is labeled by the atomic symbol followed by a unique atom descriptor. For example, $\mathbf{r}_{c\alpha 2}$, refers to the position of one of the α-carbons. The fit parameters associated with each atom site are labeled similarly; for example, c_1^α, is the first parameter associated with a fit function centered on one of the α-carbon atoms. For fit functions that are not associated with atomic sites on the molecular frame, we denote the position vectors as $\mathbf{r}_{a\{site\}}$ where $\{site\}$ is a label to indicate its location. We have chosen the following notation for the off-molecule sites: ao(1&2) refer to the two features near the oxygen atom, ac(1&2) refer to the features near the β-carbon atoms, aa refers to the aft feature on the molecular axis, and af labels the feature above the oxygen atom on the molecular axis (cf. Figs. 3 & 4).

One of our chief motivations in our choice of fit function was to try to keep physical insight into the origins of the effective potential. For example, we expect the effective potential associated with each of the atom sites to have some local r^{-1} character since the core electrons do not perfectly shield the nuclei from the excess electron; indeed, the damped r^{-1} form is the dominant characteristic of the effective potential near the H atoms. In addition, the rapidly decaying repulsive spike on the oxygen atom visible in Figure 3A also fits well to an r^{-1} form; as discussed above, surrounding this spike is an attractive well that we found was adequately fit with a 4th-order polynomial in each direction. The angled p-like features centered on the carbon sites seen in Figure 3B fit well to p-like cartesian Gaussians. One of the key features of the effective potential that made it so difficult to fit is the fact that the general decay of the potential is different in the molecular plane versus normal to it; thus, the single biggest improvements came by allowing each the fit functions to have different decay constants in different directions. This anisotropy is particularly apparent in the features located to either side of the oxygen atom, which fit quite well to Gaussians but with decay constants that differ by a factor of $\sim$2 in different directions. The other off-atom sites were similarly well treated with anisotropic Gaussians.

Figure 5A shows the fit, with the parameters quoted in Table I, for a cut parallel to the THF molecular plane but 0.16 a_0 above it; this is the same cut for which the exact effective potential is shown in Figure 3A. Figure 5B plots the difference between the fit and the exact potential in this plane. Although residual features are clearly visible in Fig. 5B, the amplitude of the difference is quite small relative to the size of the features in the exact potential. The only region where we are somewhat unsatisfied with the quality of the fit is around the carbon atoms, but we found it difficult to improve the fit without the addition of many more functional parameters. The supplementary information presents the values of the exact effective potential calculated from -10 a_0 to 10 a_0 on both a 64^3 and a 128^3 evenly-spaced cubic grid for any researchers who wish to perform alternate fits or who wish to investigate cuts of the exact potential that we have not shown in this paper.

IV. CONCLUSIONS

In this paper, we have presented a computational methodology for calculating the exact effective potential for molecular systems via the solution to Eqns. 7 and 9. We have illustrated this methodology by calculating the THF-e$^-$ effective potential, which is one of the most complex systems for which an exact potential has been calculated. In addition, with our computationally efficient formalism, such calculations lie on the low end of computational feasibility; the full calculation for the THF-e$^-$ effective potential presented here took less than 10 s on a somewhat modest serial processor. In order to use the effective potential in mixed quantum/classical simulations, we also presented a fit of the exact potential.

Given that this method can be applied to much more complex systems, there are a range of possibilities for future work. One possibility is that this formalism can be readily extended to include corrections to the frozen core approximation in a perturbative, on-the-fly fashion [12]. Obviously, this formalism could be used to calculate effective potentials for much larger molecules. Since the potential energy evaluation of the pseudo-orbital is entirely excluded from such calculations, the limit to the size of the system is bounded only by the ability to obtain the original core and valence electron wavefunctions for the system of interest.

V. ACKNOWLEDGEMENTS

This work was supported by the National Science Foundation under grant number CHE-0240776. B.J.S. is a Camille Dreyfus Teacher-Scholar. We gratefully acknowledge UCLA Academic Technology Services for the use of its Hoffman Cluster and other computational resources.

---

[1] W. E. Pickett, Comp. Phys. Rep. **9**, 115 (1989).

[2] M. J. Bedard-Hearn, R. E. Larsen, and B. J. Schwartz, J. Chem. Phys. **122**, 134506 (2005).

[3] C. J. Smallwood, W. B. Bosma, R. E. Larsen, and B. J. Schwartz, J. Chem. Phys. **119**, 11263 (2003).

[4] K. F. Wong and P. J. Rossky, J. Phys. Chem. A **105**, 2546 (2001).

[5] W. S. Sheu and P. J. Rossky, J. Phys. Chem. **100**, 1295 (1996).

[6] D. F. Coker and B. J. Berne, *Quantum Calculations of Excess Electrons in Disordered Media, Excess Electrons in Dielectric Media* (CRC Press, 1991).

[7] L. Szasz, *Pseudopotential Theory of Atoms and Molecules* (Wiley Interscience, 1985).

[8] J. C. Phillips and L. Kleinman, Phys. Rev. **116**, 287 (1959).

[9] J. Schnitker and P. J. Rossky, J. Chem. Phys. **86**, 3462 (1987).

[10] I. Abarenkov and V. Heine, Phil. Mag. **12**, 529 (1965).

[11] R. W. Shaw, Phys. Rev. **174**, 769 (1968).

[12] C. J. Smallwood and B. J. Schwartz, manuscript in preparation (2005).

[13] L. Turi, M. P. Gaigeot, N. Levy, and D. Borgis, J. Chem. Phys. **114**, 7805 (2001).

[14] I. B. Martini, E. R. Barthel, and B. J. Schwartz, J. Chem. Phys. **113**, 11245 (2000).

[15] I. B. Martini and B. J. Schwartz, Chem. Phys. Lett. **360**, 22 (2002).

[16] E. R. Barthel, I. B. Martini, and B. J. Schwartz, J. Chem. Phys. **112**, 9433 (2000).

[17] E. R. Barthel, I. B. Martini, and B. J. Schwartz, J. Phys. Chem. B **105**, 12230 (2001).

[18] E. R. Barthel and B. J. Schwartz, Chem. Phys. Lett. **375**, 435 (2003).

[19] I. B. Martini, E. R. Barthel, and B. J. Schwartz, Pur. App. Chem. **76**, 1809 (2004).

[20] I. B. Martini, E. R. Barthel, and B. J. Schwartz, J. Am. Chem. Soc. **124**, 7622 (2002).

[21] Z. H. Liu and B. J. Berne, J. Chem. Phys. **99**, 9054 (1993).

[22] M. H. Cohen and V. Heine, Phys. Rev. **122**, 1821 (1961).

[23] L. Turi and D. Borgis, J. Chem. Phys. **117**, 6186 (2002).

[24] A. Szabo and N. Ostlund, *Modern Quantum Chemistry* (Dover Publications, New York, 1996).

[25] M. A. Morrison and L. A. Collins, Phys. Rev. A **17**, 918 (1978).

[26] e. a. Frisch, M. J., Tech. Rep., Gaussian, Inc. (1998).

[27] J. Chandrasekar and W. L. Jorgensen, J. Chem. Phys. **77**, 5073 (1982).

[28] E. Anderson, Z. Bai, J. Bischof, J. Demmel, J. Dongarra, A. Du Croz, A. Greenbaum, S. Hammarling, A. McKenney, and D. Sorenson, Tech. Rep., Computer Science Department, University of Tennessee, Knoxville, TN (1990).

$U_{fit}(\mathbf{r}) = \left\{ \begin{array}{llllll} & U_o & + U_{c\alpha 1} & + U_{c\alpha 2} & + U_{c\beta 1} & + U_{c\beta 2} \\ + & U_{h\alpha 1} & + U_{h\alpha 2} & + U_{h\alpha 3} & + U_{h\alpha 4} & + U_{h\beta 1} \\ + & U_{h\beta 2} & + U_{h\beta 3} & + U_{h\beta 4} & + U_{ao} & + U_{ao} \\ + & U_{ac} & + U_{ac} & + U_{aa} & + U_{af} & \end{array} \right.$			
$U_o(\mathbf{r}-\mathbf{r_o}) = \begin{array}{ll} & \big(o_1(x-x_o)^4 + o_2(y-y_o)^4 + o_3(z-z_o)^4 - o_4\big) \\ \times & exp\left(-\left[o_5(x-x_o)^2 + o_6((y-y_o)^2 + (z-z_o)^2)\right]\right) \\ + & o_7 \frac{e^{-o_8(\mathbf{r}-\mathbf{r_o})^2}}{\vert\mathbf{r}-\mathbf{r_o}\vert} \end{array}$			
$o_1 = 2.8926$	$o_2 = 0.1017$	$o_3 = 1.9379$	$o_4 = 4.1887$
$o_5 = 1.0552$	$o_6 = 1.2853$	$o_7 = 9.4147$	$o_8 = 23.4135$
$U_{c\alpha}(\mathbf{r}-\mathbf{r_{c\alpha}}) = \begin{array}{ll} & c_1^\alpha \left[(y-y_{c\alpha}) + c_2^\alpha(z-z_{c\alpha})\right] \\ \times & exp\left(-\left[c_3^\alpha(x-x_{c\alpha})^2 + c_4^\alpha((y-y_{c\alpha})^2 + (z-z_{c\alpha})^2)\right]\right) \\ - & c_5^\alpha \frac{1}{\vert\mathbf{r}-\mathbf{r}_{c\alpha}\vert} + c_6^\alpha exp\left[-c_7^\alpha(\mathbf{r}-\mathbf{r}_{c_\alpha})^4\right] \end{array}$			
$c_1^\alpha = 62.6462$	$c_2^\alpha = 0.1426$	$c_3^\alpha = 7.9044$	$c_4^\alpha = 7.9516$
$c_5^\alpha = 0.3147$	$c_6^\alpha = 6.3821$	$c_7^\alpha = 34.2773$	
$U_{c\beta}(\mathbf{r}-\mathbf{r_{c\beta}}) = \begin{array}{ll} & c_1^\beta \left[(y-y_{c\beta}) + c_2^\beta(z-z_{c\beta})\right] \\ \times & exp\left[-\left(c_3^\beta(x-x_{c\beta})^2 + c_4^\beta((y-y_{c\beta})^2 + (z-z_{c\beta})^2)\right)\right] \\ - & c_5^\beta \frac{1}{\vert\mathbf{r}-\mathbf{r}_{c\beta}\vert} + c_6^\beta e^{-c_7^\beta(\mathbf{r}-\mathbf{r}_{c\beta})^4} \end{array}$			
$c_1^\beta = 13.3107$	$c_2^\beta = 1.3455$	$c_3^\beta = 5.3624$	$c_4^\beta = 4.4085$
$c_5^\beta = 0.3033$	$c_6^\beta = 1.4495$	$c_7^\beta = 7.8897$	
$U_{h\alpha}(\mathbf{r}-\mathbf{r_{h\alpha}}) = -h_1^\alpha \frac{exp\left[-h_2^\alpha(\mathbf{r}-\mathbf{r}_{h\alpha})^2\right]}{\vert\mathbf{r}-\mathbf{r}_{h\alpha}\vert} + h_3^\alpha exp\left[-h_4^\alpha(\mathbf{r}-\mathbf{r}_{h\alpha})^2\right]$			
$h_1^\alpha = 0.8357$	$h_2^\alpha = 0.8769$	$h_3^\alpha = 0.2657$	$h_4^\alpha = 0.0852$
$U_{h\beta}(\mathbf{r}-\mathbf{r_{h\beta}}) = -h_1^\beta \frac{exp\left[-h_2^\beta(\mathbf{r}-\mathbf{r}_{h\beta})^2\right]}{\vert\mathbf{r}-\mathbf{r}_{h\beta}\vert} + h_3^\beta exp\left[-h_4^\beta(\mathbf{r}-\mathbf{r}_{h\beta})^2\right]$			
$h_1^\beta = 0.7861$	$h_2^\beta = 0.9584$	$h_3^\beta = 0.1362$	$h_4^\beta = 0.0359$
$U_{ao}(\mathbf{r}-\mathbf{r_{ao}}) = a_1^o exp\left[-\left(a_2^o(x-x_{ao})^2 + a_3^o(y-y_{ao})^2 + a_4^o(z-z_{ao})^2\right)\right]$			
$a_1^o = 2.7673$	$a_2^o = 1.0552$	$a_3^o = 0.5211$	$a_4^o = 0.7436$
$U_{ac}(\mathbf{r}-\mathbf{r_{ac}}) = a_1^c exp\left[-\left(a_2^c(x-x_{ac})^2 + a_3^c((y-y_{ac})^2 + (z-z_{ac})^2)\right)\right]$			
$a_1^c = 0.9996$	$a_2^c = 0.6810$	$a_3^c = 0.3058$	
$U_{aa}(\mathbf{r}-\mathbf{r_{aa}}) = \begin{array}{ll} & a_1^a exp\left[-\left(a_2^a(x-x_{aa})^2 + a_3^a((y-y_{aa})^2 + (z-z_{aa})^2)\right)\right] \\ - & a_4^a exp\left[-\left(a_5^a(x-x_{aa})^2 + a_6^a((y-y_{aa})^2 + (z-z_{aa})^2)\right)\right] \end{array}$			
$a_1^a = 11.7043$	$a_2^a = 0.5978$	$a_3^a = 0.1703$	
$a_4^a = 10.7099$	$a_5^a = 0.5994$	$a_6^a = 0.1597$	
$U_{af}(\mathbf{r}-\mathbf{r_{af}}) = a_1^f exp\left[-\left(a_2^f(x-x_{af})^2 + a_3^f(y-y_{af})^2 + a_4^f(z-z_{af})^2\right)\right]$			
$a_1^f = 0.4472$	$a_2^f = 0.0443$	$a_3^f = 0.0379$	$a_3^f = 0.2579$

TABLE I: **Functional Form and Parameters of the Fit to the Exact e$^-$–THF Effective Potential.** The 47-parameter fit has functional contributions centered on 19 different sites. The functional and parameter notations are explained in the text. For the parameters given here, the distances are in Bohr radii and the energies are in Hartrees.

Figure Captions:

FIGURE 1: Hydrogen-optimized Planar THF Structure used in this Work. The bond distances are given in Angstroms (Å) and angles are in degrees.

FIGURE 2: Correcting the Divergence of THF-e$^-$ Effective Potential at Large Distances Due to the Choice of a Gaussian Basis Set. The solid curve in Panel A shows the quadratic divergence of the localized potential calculated via Eqns. 6 & 7 that results from choosing the 6-31++g basis set; the 1-D cut displayed is along a line perpendicular to the molecular plane that intersects the point (0.16 a_0,-1.42 a_0 relative to the THF center-of-mass. The dashed curve in Panel A shows the Coloumb potential of the LUMO along this same cut, which provides the correct asymptotic behavior of the effective potential. Panel B shows the melded potential, joined at the intersection closest to the THF center of mass, as described in the text; note that the kink introduced by the melding procedure is small compared to the natural features of the effective potential.

FiGURE 3: 2-D Cuts of the Exact Effective e-THF Potential Parallel to the Molecular Plane. The magnitude of the potential in each panel, given by the color scale, is in Hartrees and the spatial axes have units of Bohr radii. The schematic THF molecule drawn in the top left corner of each panel illustrates the perspective of the cut as well as the cartesian axis labels used for the fit described in Table I. The cut in Panel A is 0.16 a_0 above the molecular plane; the cut in Panel B is 0.48 a_0 above the molecular plane. Note that the color scale is not the same in the two panels, and that the magnitude of the potential decays quickly with increasing distance from the molecular plane.

FIGURE 4: 2-D Cut of the Exact Effective e-THF Potential Perpendicular to the Molecular Plane. As with Fig. 3, the color scale gives the potential energy in Hartrees and the distance units are in Bohr radii. The viewing perspective of this cut is indicated in the top left corner, where the vertical bar near the β-hydrogens represents the plane in which the potential is shown. The strong effect of the hydrogen atoms is clearly visible as the four attractive centers above and below the THF plane.

FIGURE 5: Fit to the Exact e$^-$–THF Effective Potential. Panel A shows a 2-D cut of the 47-parameter fit (see Table I and text) parallel to the THF molecular plane and 0.16 a_0 above it; this is the same cut for which the exact effective potential is shown in Figure 3A. Panel B shows the residuals of the fit; i.e. the difference between Figs. 5A and 3A.

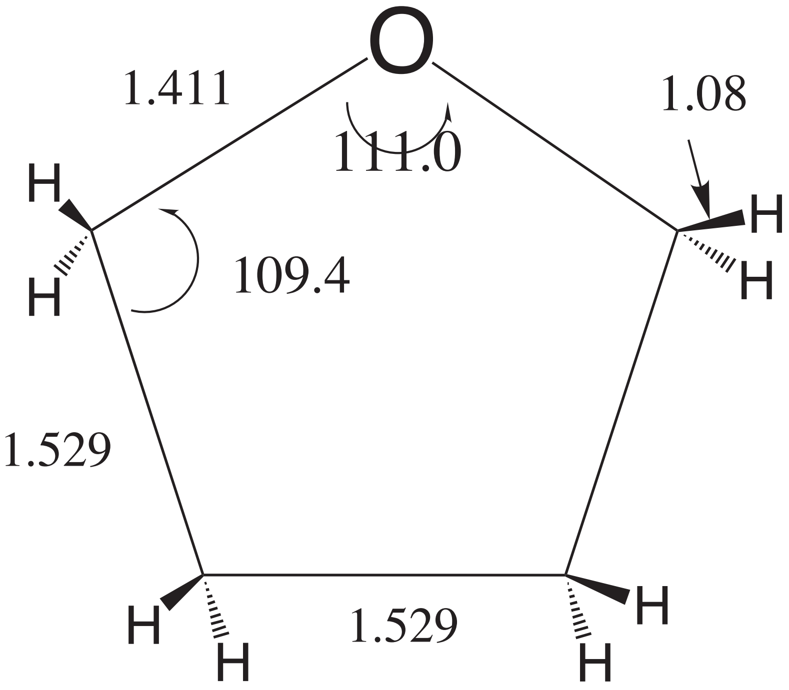

Smallwood et al., JCP, Figure 1

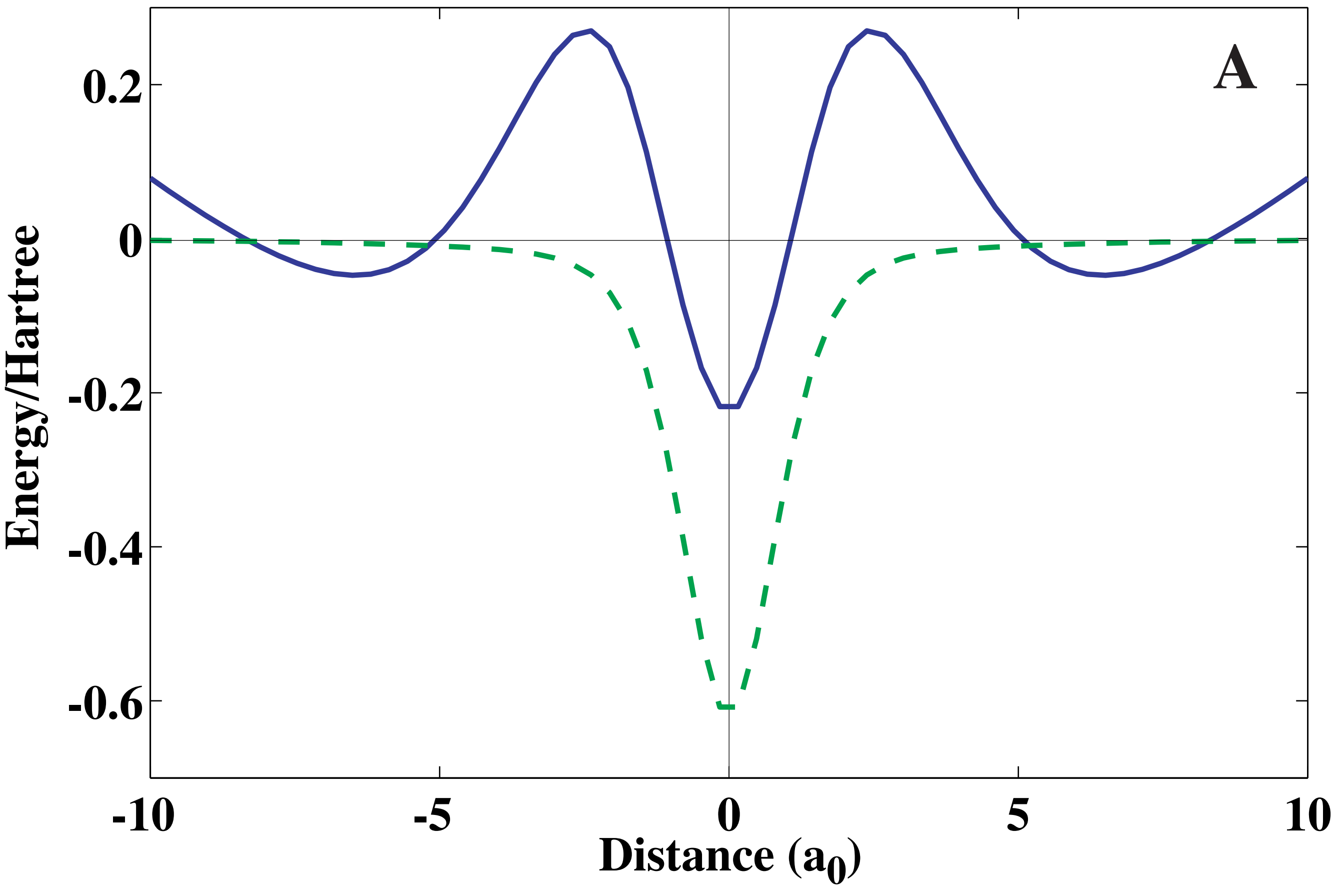

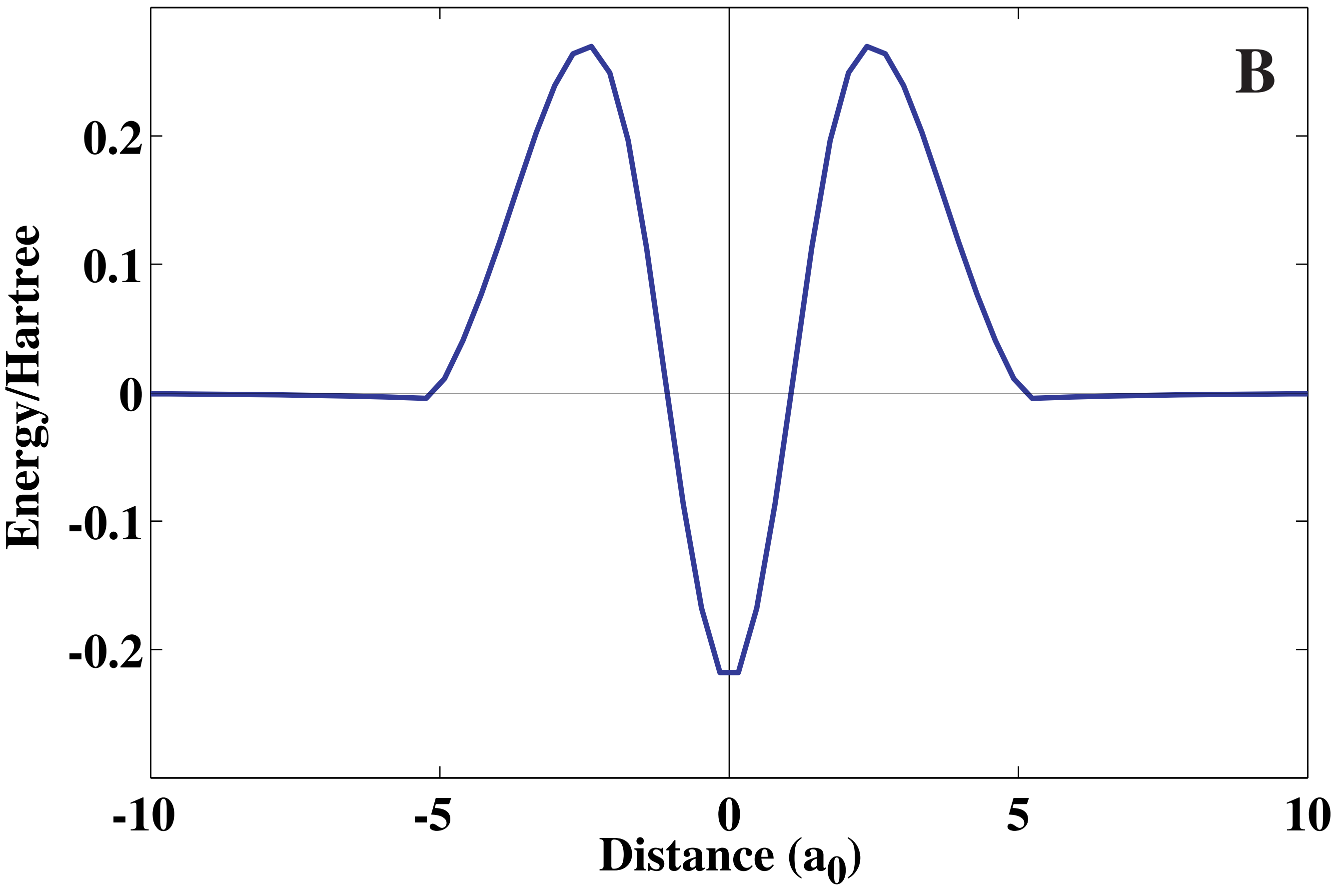

Smallwood et al., JCP, Figure 2

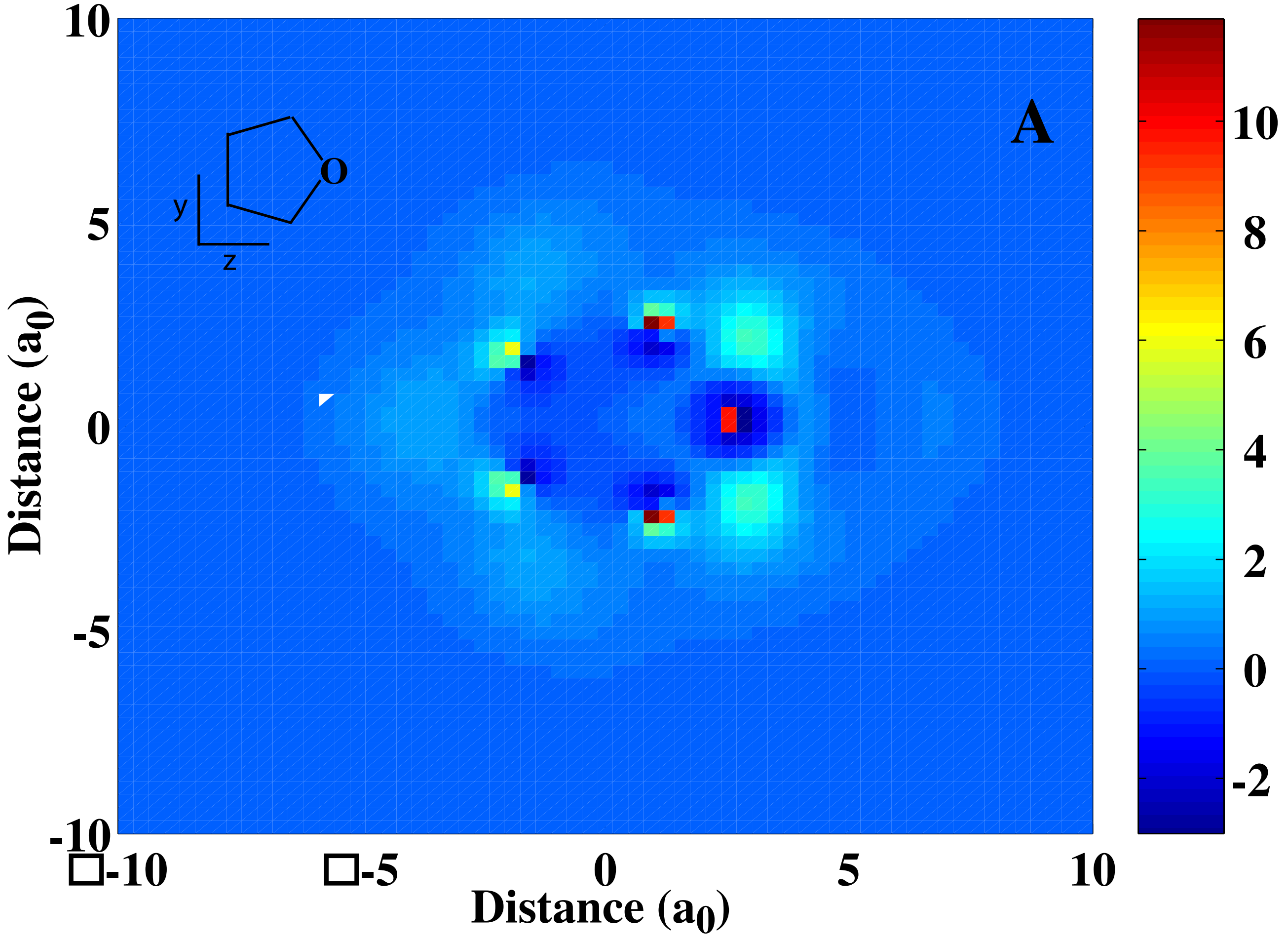

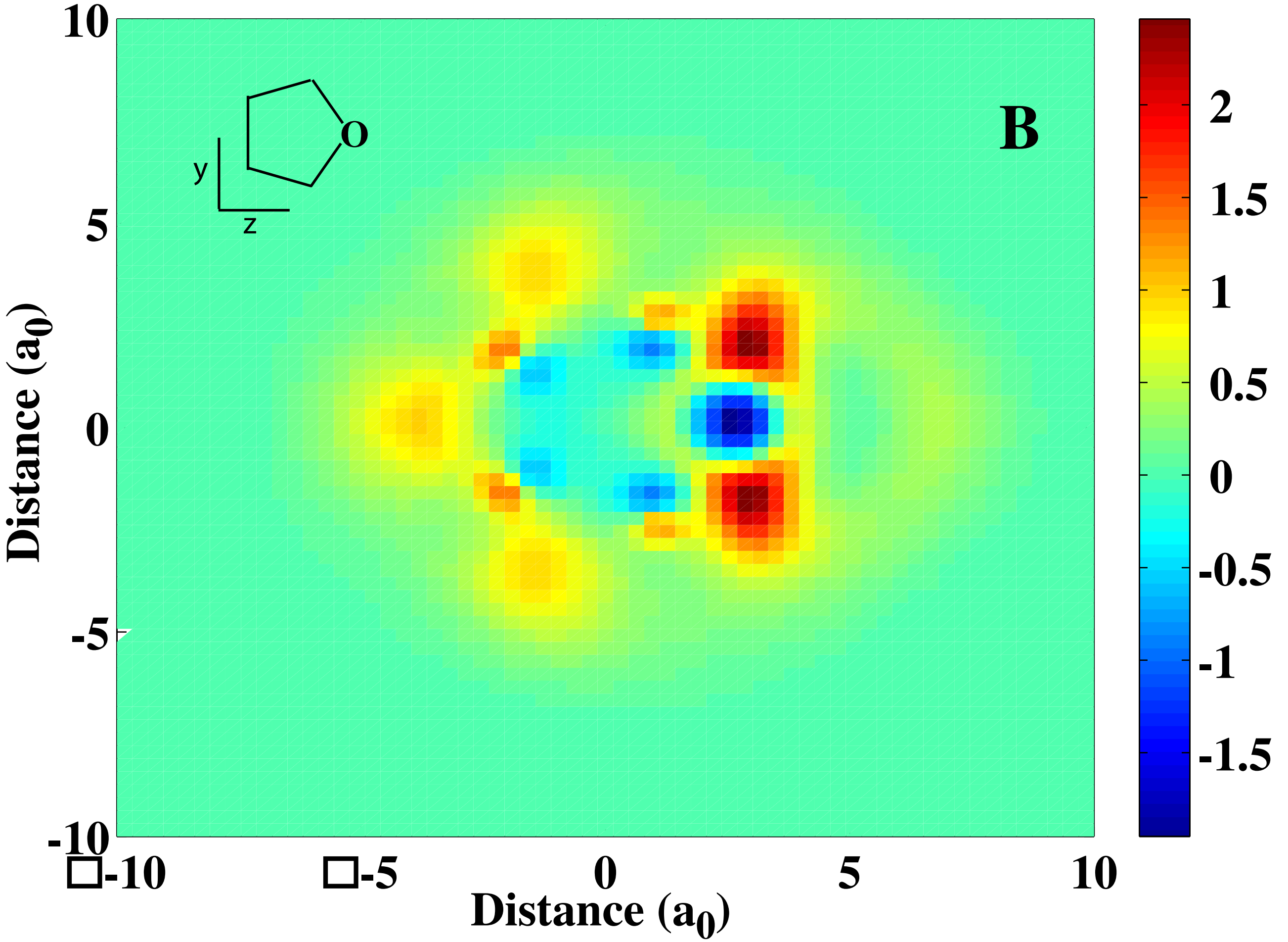

Smallwood et al., JCP, Figure 3

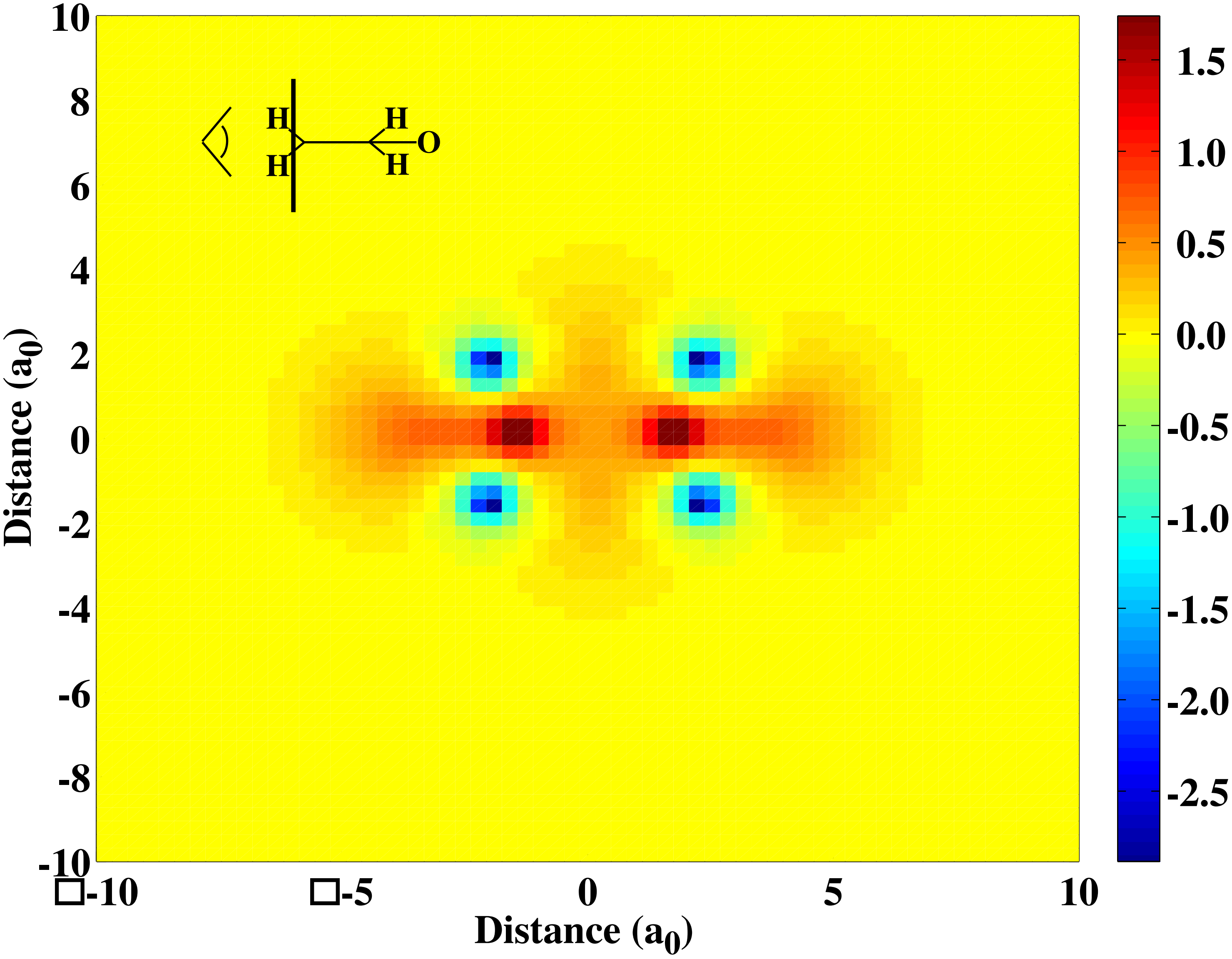

Smallwood et al., JCP, Figure 4

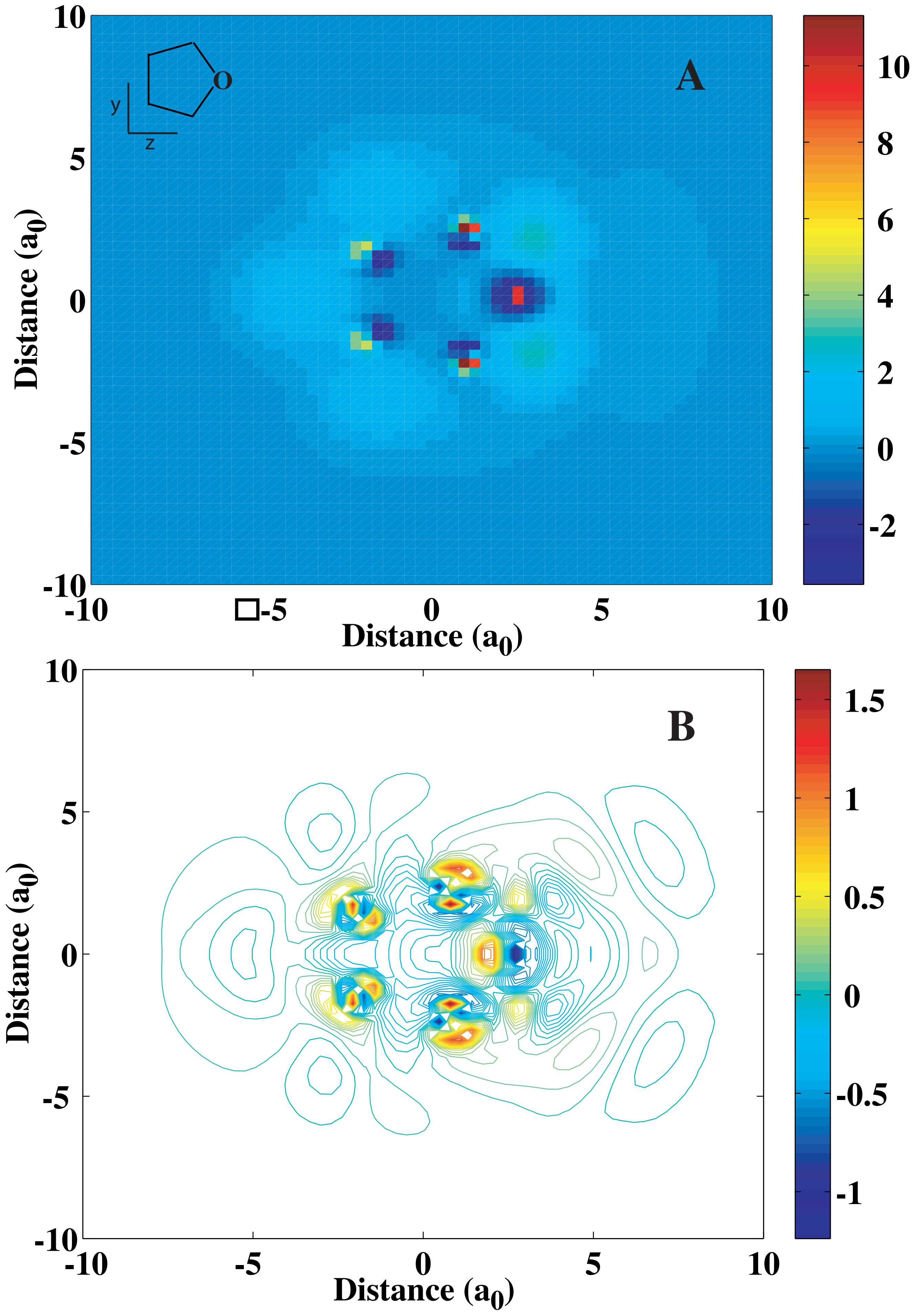

Smallwood et al., JCP, Figure 5